Suppression of Richtmyer-Meshkov Instability via Special Pairs of Shocks and Phase Transitions

W. J. Schill, M. R. Armstrong, J. H. Nguyen, D. M. Sterbentz, D. A. White, L. X. Benedict, R. N. Rieben, A. Hoff, H. E. Lorenzana, J. L. Belof, B. M. La Lone, and M. D. Staska

Phys. Rev. Lett. **132**, 024001 — Published 9 January 2024

DOI: 10.1103/PhysRevLett.132.024001

Suppression of Richtmyer-Meshkov instability via special pairs of shocks and phase transitions

W. J. Schill,* M. R. Armstrong, J. H. Nguyen, D. M. Sterbentz, D. A. White, L. X. Benedict, R. N. Rieben, A. Hoff, H. E. Lorenzana, and J. L. Belof
Lawrence Livermore National Laboratory, 7000 East ave, Livermore, CA 94550, USA.

B. M. La Lone and M. D. Staska
Special Technologies Laboratory 5520 Ekwill St b, Santa Barbara, CA 93117

(Dated: November 14, 2023)

The classical Richtmyer-Meshkov instability is a hydrodynamic instability characterizing the evolution of an interface following shock loading. In contrast to other hydrodynamic instabilities such as Rayleigh-Taylor, it is known for being unconditionally unstable: regardless of the direction of shock passage, any deviations from a flat interface will be amplified. In this article, we show that for negative Atwood numbers, there exist special sequences of shocks which result in a nearly perfectly suppressed instability growth. We demonstrate this principle computationally and experimentally with stepped fliers and phase transition materials. A fascinating immediate corollary is that in specific instances a phase transitioning material may self-suppress RMI.

The classical Richtmyer-Meshkov instability (RMI) is a hydrodynamic instability characterizing the evolution of an interface following shock loading. In the case of a shock passing from a heavy material to a light material, the evolution of the interface follows a standard behavior, valleys evolve into peaks or *jets* and the initial peaks evolve into valleys. RMI occurs in many scientific areas [1–5] including laser driven inertial confinement fusion (ICF) [6, 7] such as is pursued at the National Ignition Facility (NIF). RMI is a critical limiting physical mechanism controlling the onset of mix which ultimately may degrade ICF performance [7, 8]; thus, development of methodologies to suppress growth of RMI can be viewed as one of the key bottlenecks to development of abundant clean energy via fusion. A productive description of RMI in terms of the vorticity field (cf. [9]) was introduced in [10–13]. In this conception of the instability physics, the passage of the shock through the interface deposits vorticity at the interface via the baroclinic mechanism. The variation in the sign of the vorticity arising from the non-planarity of the interface gives rise to the instability.

In this article, we advance the following conjecture: for a heavy-light interface loaded by two shocks in sequence, owing to the fact that the interface shape inverts (i.e. valleys become peaks and peaks become valleys), there will be a special time delay between the shocks such that the vorticity deposited by the second shock will be nearly equal and opposite the vorticity deposited by the first shock; thereby canceling (potentially to zero) and leaving the interface stable. The proposed RMI suppression principle which we refer to as *double shock* is illustrated in Fig. 1. Of course, virtually no interface in application is a perfect sinusoid [14, 15]; we derive a formula for optimal shock timing corresponding to arbitrary groove shapes. This principle is extremely effective in suppressing RMI from differently shaped grooves.

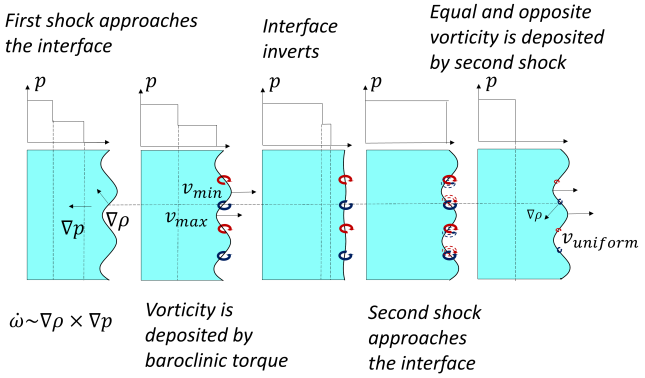

FIG. 1. The proposed mechanism of suppresses RMI via shock timing. A double shock wave propagates depositing vorticity at the interface with a specific timing wherein the second vorticity deposition cancels the first due to the inversion of the wave profile.

The classical paper by Richtmyer [16] modified earlier work due to Taylor [17] to derive, for a single sinusoidal surface perturbation of wavenumber k, the velocity of amplitude growth $\bar{v} = k\Delta u A^+ a_0$, where Δu is the jump in particle velocity arising from the shock, $A^+ = (\rho_{\text{downstream}} - \rho_{\text{upstream}})/(\rho_{\text{downstream}} + \rho_{\text{upstream}})$ is the Atwood number, and a_0 is the initial amplitude.

We now suppose that the effects of two shocks in sequence may be superposed linearly giving the perturbation amplitude velocity

$$v(k) = v_1(k) + v_2(k) \ , \tag{1}$$

* schill1@llnl.gov

where

$$v_i(k) = k\Delta u_i A^+ a_{i,0}(k) \ , \tag{2}$$

where the index $i = 1, 2$ denotes the first or second shock. Note the dependence on wavenumber k. We observe that under a constant velocity following the first shock, the initial amplitude for the second shock will be

$$a_{2,0}(k) = v_1(k)t + a_{1,0}(k) \ . \tag{3}$$

Now, we investigate whether there is a pair of shocks for which the amplitude growth is minimized. Minimizing $\sum_k |v(k)|^2$, and solving equations (1),(2), and (3) we obtain an expression for the delay time between the two shocks as a function of the jumps in velocity

$$t = -\frac{1}{A^+}\left(\frac{1}{\Delta u_1} + \frac{1}{\Delta u_2}\right) c_g \ , \tag{4}$$

where c_g is a geometric prefactor accounting for the effects of multiple wavenumbers

$$c_g = \frac{\sum_k^\infty k^3 a_{1,0}^2(k)}{\sum_k^\infty k^4 a_{1,0}^2(k)} \ . \tag{5}$$

Equation (4) has the simple interpretation of the harmonic average of the particle velocity jumps with a prefactor coming solely from the Atwood number and the spectral content of the interface via c_g. Evidently, for $A^+ < 0$, this equations yields $t > 0$. We mention that, in the special case of a single wavenumber, $c_g = 1/k$ and the velocity arrests completely; this phenomena was first pointed out by [18], labeled 'freeze-out', and a formula which is a special case of (4) was presented.

Evidently, c_g depends on the spectral content of the initial interface via $a_{1,0}(k)$. We suppose that $a_{1,0}(k) \propto k^{-\alpha}$ for $k \leq k_{\rm cut}$ and $a_{1,0}(k) \propto k^{-\beta}$ for $k > k_{\rm cut}$. Taking α to be a small integer and β to be large provides a simple prototype for many realistic interfaces wherein the small scale features are much smoother below some lengthscale; see [19] for some examples of real ICF capsules with power-law dependence in the spectrum of the capsule surface profile. Also, RMI effects of large wavenumbers may be regularized out by effects like strength, viscosity, or non-linearity. In Fig. 2(A), the geometric factor c_g decreases with and the instability growth velocity increases with $k_{\rm cut}/k_0$ for $\alpha = 2, 3, 4$. The case of $\alpha = 2$ is a prototype for an interface with sharp features such as a v-groove; the case of $\alpha \geq 4$ would correspond to a highly smooth interface where the spectral content decays rapidly with increasing wavenumber. Evidently, the jetting suppression is substantial particularly for k_{cut} not too large or for $\alpha > 2$. In light of the case of $k_{\rm cut}/k_0 = 1$, we observe that $c_g k_0$ can be interpreted as the fractional reduction in delay time between the two shock waves relative to the optimal delay time for an interface with a single wave number.

To understand the shock structure, we consider a stepped flier plate shown in Fig. 2 (B). The stepped flier consisting of heavy (*navy*) and light (*gray*) materials strikes the target (*light gray*). In addition to the launching a shockwave into the target, a shockwave propagates through the stepped flier; this reflects from the heavy material launching the second shock into the target. We remark that this 1D x-t diagram is quite a bit simpler than the 2D RMI picture we have thus far introduced however we can obtain a surprising amount of insight regarding the shock strengths and timing. The classical jump condition from the balance of momentum (neglecting dissipative effects) is $[|p|] - c_s[|\rho u|] = 0$, where p is the pressure, ρ is the density, and u is the particle velocity. For simplicity, we suppose that at the particle

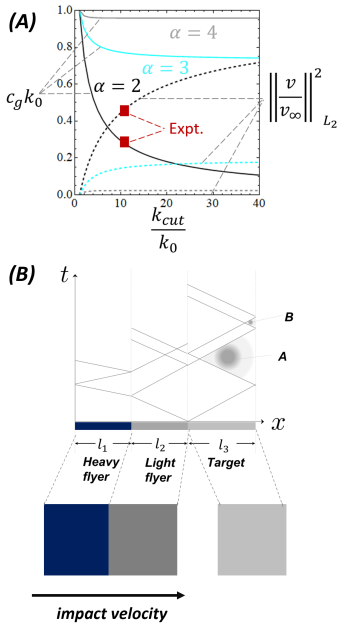

FIG. 2. (A) We show $c_g k_0$ and the velocity (normalized by by unmitigated jet velocity, v_∞) of the suppressed jet as a function of properties of the spectral content of the original interface. Spectral character of our experimental samples obtained via surface profilometry is shown in red. (B) We sketch a notional x-t diagram for an experimental design using stepped fliers. This shows the propagation of shockwaves through the stepped flyer. We denote the particle velocities in space-time regions A and B respectively.

velocities experienced by the target and first flier, the shock speed c_s is nearly constant. Further, we assume that the changes in density are not too large. With these assumptions, it is easy to develop explicit expressions for the particle velocity following the arrival of the first and second shock. The particle velocity of the first u_A and second shock u_B, respectively, are given by

$$u_A = \frac{2\rho_2 c_{s2}}{c_{s3}\rho_3 + \rho_2 c_{s2}} u_0 \ , \tag{6}$$

and

$$\frac{u_B}{u_A} = \frac{\left(3\ c_{s3}c_{s1}\rho_3\rho_1 - c_{s3}\rho_2\rho_3 c_{s2} + c_{s1}\rho_2\rho_1 c_{s2} + \rho_2^2 c_{s2}^2\right)}{(c_{s3}\rho_3 + \rho_2 c_{s2})(c_{s1}\rho_1 + \rho_2 c_{s2})}\ , \tag{7}$$

where ρ_i and c_{si} are the density and shock speed of the ith material indexed from left to right in Fig. 2. If the constant shock speed or small density change assumption is omitted, this still may be (analytically) solvable in certain cases, however the expressions become significantly more complex. An additional complexity here is that the topology of the intersecting shock waves in Fig. 2 may change depending on thicknesses and shock speeds; thus, the specific expression may actually change. Importantly though, the behavior of the stepped release velocity is somewhat robust with respect to these kinds of changes.

We estimate the time delay between the first and second shocks as $\tau = 2l_2/c_{s2}$ where l_2 is the thickness of the first-shock flier. Equating this time delay and (4), we obtain an expression for the thickness l_2 which will best suppress the RMI.

We now consider scenarios in which shock-induced phase transitions can suppress RMI. In such a case, the material has multiple wave-speeds; the resulting behavior can be complex and difficult to treat analytically. To make progress, we suppose that there is a single wavespeed in both the parent and daughter materials. This is a coarse assumption as in a real material the behavior will depend on compression and dissipative effects; however, it is conceptually powerful and facilitates understanding of the suppression mechanism. To have a stable multi-wave structure, we must have the condition that the lower pressure phase has a faster wave speed than the higher pressure phase: $c_1^2 \geq c_2^2$ [20]. If this condition does not hold, the materials is overdriven and the high pressure phase shock speed will overtake the low pressure shock. Given a certain sample size l, it is easy to see that the time delay between the arrival of the first and second waves is $\tau = l\left(c_1^{-1} - c_2^{-1}\right)$. Equating this with (4), we have a relationship between the length of the phase transition material and the wavenumber of the interface. Similar to the preceding stepped flier discussion, we give simple estimates of the release velocity in the supplemental material. Even in the presence of complicating factors, the qualitative behavior outlined here will hold suggesting that a combination of experimental geometry and properties of the phase transition will lead to the self-suppression of RMI of a specific wavelength.

We now present computational and experimental results which support the proposed RMI suppression strategies. For our simulations, we use the high order production multiphysics code MARBL [21–24]. For targets simulated here, we have used the equation of state LEOS 5060 for the PMMA target and SESAME-2140 for the iron target. For the iron target, we used an elastic-linearly-plastic model with yield strength of 65 MPa and with a linear hardening coefficient of 10 GPa; we remark that this is an exceptionally simple model and discrepancies between the simulation and the experiment are likely attributable to real complexities in the hardening behavior. The first simulation in Fig. 3 (A) is driven by a double shock well matched by our theory to the groove size and the second is a control case with a single shock selected to drive a free flat surface to the same particle velocity as the double shock case. Evidently, the suppression is very strong with the jet length arresting following passage of the second shock in contrast to a standard shock loading where the jet continues to grow linearly. In the case driven by a double shock, the vorticity just upstream of the forming jet undergoes a precipitous drop as the second wave passes directly preceding the arrest of the jetting behavior.

In Fig. 3 (B), jetting varies with groove size for a shock wave passing through an iron target; iron undergoes a phase transition from α (BCC) phase to ϵ (HCP) phase at a pressure of about 13.8 GPa which exhibits a large volume change yielding the double shock-wave structure in this case. The analysis of instability suppression is complicated by the fact that the strength of iron is substantial; the yield strength itself will cause the jet to arrest. We must seek metrics which control for the sensitivity of arrest length to yield strength and demonstrate the sensitivity to double shock. As shown in [25], in the absence of a phase transition, one expects the product of asymptotic jet length times wave-number to exhibit this property; specifically, it scales like $\rho\dot{\xi}_0^2/Y$ where $\dot{\xi}_0$ is the initial perturbation velocity and is consequently independent of scale. In our case, the asymptotic limit of jet length per wave length shows variation which would not occur in the absence of a phase transition. We further extend our analytic approach to include strength following [25] by adding a constant deceleration leading to a contribution to the instability growth rate of $v_y = CkYt/\rho$ where C is a constant of order unity, Y is the flow strength, t is the time since the perturbation reached max velocity, and ρ is the density. This is plotted in cyan and, given the extreme simplicity of the model, agrees quite closely. We mention that the strain rate will affect the behavior of the jetting as measured by this metric; however, given the variation in groove sizes considered here, there is unlikely to be a substantial effect. The arrest length to wave length ratio decreases substantially as the wavelength is brought into alignment with the drive-timing provided by the experimental design. This demonstrates that the double shock principle, in the context of phase transitions, suppresses jetting.

We now report the results of two gas-gun experiments supporting the efficacy of the double shock principle. These experiments were conducted at Special Technologies Laboratory on their single-stage gas gun. The basic fact that we wish to exploit is that for a given two shock structure the amplitude growth rate should depend, according to our simple theory, on the wave number. Thus, we specifically design dynamic experiments with two grooves, one matching the drive and one significantly different where the jetting structure is preserved.

Experiment 1 used a 39 mm diameter stepped flier

(4mm thick tantalum back plate and 2.6 mm thick PMMA front) launched at 2.3 mm/μs at a 2mm thick PMMA target with a 0.6 mm deep 90 degree groove and a 2.4 mm deep 90 degree groove. Experiment 2 used a 38 mm diameter 8mm thick aluminum flier at = 1.315 mm/μs striking a 6 mm iron target with 0.6 and 2.4 mm deep 90 degree grooves. In both cases, the experiments are designed so that jetting from the smaller groove should be suppressed and jetting from the larger groove will not be well suppressed.

In Fig. 4, we show radiographs (left) of the static and dynamic radiographs of the two experiments as well as the velocimetry data (right) for the two experiments. In the upper left of Fig. 4, the double shock experiment shows that the smaller groove (the groove well-matched to be suppressed) exhibits a strongly suppressed jet while the larger groove exhibits a standard jet. We remark that the smaller groove exhibits small secondary jets on the sides of the original grooves; we have observed that this occurs when the second shock arrives a little bit after optimal timing. Experiment 2 in the lower left of Fig. 4 shows that the jetting from the smaller groove is completely suppressed whereas the larger groove still exhibits some jetting.

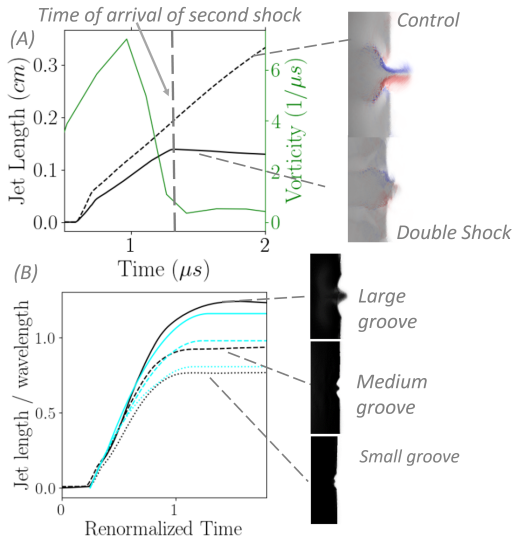

FIG. 3. Simulations are shown for (A) a stepped flyer and (B) an iron target driven by shock loading through the phase transition. In (A), the *solid* lines are from the double shock and the *dashed* lines are from the control case with a single shock selected to drive the target to an equivalent particle velocity. The asymptotic velocity of the planar free surface is virtually identical while in the double shock case, the deviation from planarity due to interface evolution is dramatically reduced. In (B), the groove size in an iron target is varied and the small groove is well-matched to the resulting double shock; evidently, the jet is minimized in this case. The theory is plotted in cyan and agrees well.

The simulations agree well with the experimental velocimetry with very simple models and no tuning of material specific parameters. In particular, we point out that the late time velocities for the small groove and the flat surface are nearly identical while the large groove velocity remains much higher. This demonstrates suppression of jetting from the smaller groove as, in the absence of a well-tuned double shock drive, the velocities of the two groove measurements should be nearly identical.

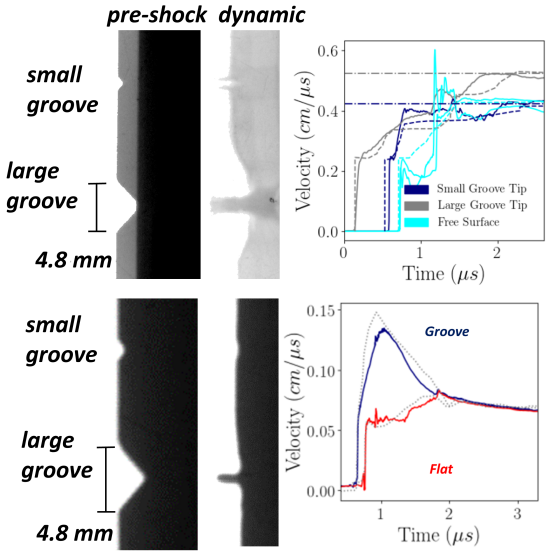

FIG. 4. Experimental radiographs for an experiment examining experiment 1 (*top left*), a stepped flyer, and for experiment 2 (*bottom left*), a phase transition in iron. We compare simulated velocity traces (solid lines) directly to experimental velocimetry data (dashed lines) and theoretical asymptotic velocity (dash-dot lines) for experiment 1 (*top right*) and experiment 2 (*bottom right*). X-ray images are taken 5 μs following impact. The experimental velocimetry measurements are shown in dashed lines and the simulated velocity histories are shown in solid lines. The jet suppression is substantial for grooves which are well matched to the double shock.

The results presented in this letter suggest that the double shock jetting suppression principle can be successfully applied in practice. In future studies, we suggest that full-field radio-graphic measurements should be made to examine in detail complex, non-sinusoidal interfaces. We suspect that a generalization to large numbers of shocks is possible, that the concept will carry over readily to curved interfaces though some of the details of the derivation will change, and that this approach could be applied to jetting suppression in ICF.

ACKNOWLEDGMENTS

This work was performed under the auspices of the U.S. Department of Energy by Lawrence Livermore Na-

tional Laboratory under Contract DE-AC52-07NA27344 and was supported by the LLNL-LDRD Program under Project No. 21-SI-006. Lawrence Livermore National Security, LLNL-JRNL-846621.

[1] Ye Zhou. Rayleigh–Taylor and Richtmyer–Meshkov instability induced flow, turbulence, and mixing. I. *Physics Reports*, 720-722:1–136, 2017.

[2] Ye Zhou. Rayleigh–Taylor and Richtmyer–Meshkov instability induced flow, turbulence, and mixing. ii. *Physics Reports*, 723:1–160, 2017.

[3] Ye Zhou et al. Rayleigh–Taylor and Richtmyer–Meshkov instabilities: A journey through scales. *Physica D: Nonlinear Phenomena*, 423:132838, 2021.

[4] Garrett Birkhoff, Duncan P MacDougall, Emerson M Pugh, and Sir Geoffrey Taylor. Explosives with lined cavities. *Journal of Applied Physics*, 19(6):563–582, 1948.

[5] Ye Zhou, Timothy T Clark, Daniel S Clark, S Gail Glendinning, M Aaron Skinner, Channing M Huntington, Omar A Hurricane, Andris M Dimits, and Bruce A Remington. Turbulent mixing and transition criteria of flows induced by hydrodynamic instabilities. *Physics of Plasmas*, 26(8):080901, 2019.

[6] Karnig O Mikaelian. Extended model for Richtmyer–Meshkov mix. *Physica D: Nonlinear Phenomena*, 240(11):935–942, 2011.

[7] Bruce A Remington et al. Rayleigh–Taylor instabilities in high-energy density settings on the national ignition facility. *Proceedings of the National Academy of Sciences*, 116(37):18233–18238, 2019.

[8] Guy Dimonte, Guillermo Terrones, Frank J Cherne, and Praveen Ramaprabhu. Ejecta source model based on the nonlinear Richtmyer-Meshkov instability. *Journal of Applied Physics*, 113(2):024905, 2013.

[9] Alexandre J Chorin. *Vorticity and turbulence*. Springer Science & Business Media, 1994.

[10] John F Hawley and Norman J Zabusky. Vortex paradigm for shock-accelerated density-stratified interfaces. *Physical review letters*, 63(12):1241, 1989.

[11] JW Jacobs and JM Sheeley. Experimental study of incompressible Richtmyer–Meshkov instability. *Physics of Fluids*, 8(2):405–415, 1996.

[12] Oleg A Likhachev and Jeffrey W Jacobs. A vortex model for Richtmyer–Meshkov instability accounting for finite atwood number. *Physics of Fluids*, 17(3):031704, 2005.

[13] Dane M Sterbentz, Charles F Jekel, Daniel A White, Sylvie Aubry, Hector E Lorenzana, and Jonathan L Belof. Design optimization for Richtmyer–Meshkov instability suppression at shock-compressed material interfaces. *Physics of Fluids*, 34(8):082109, 2022.

[14] Frank Joseph Cherne, James Edward Hammerberg, Malcolm John Andrews, V Karkhanis, and P Ramaprabhu. On shock driven jetting of liquid from non-sinusoidal surfaces into a vacuum. *Journal of Applied Physics*, 118(18):185901, 2015.

[15] Karnig O Mikaelian. Richtmyer–Meshkov instability of arbitrary shapes. *Physics of Fluids*, 17(3):034101, 2005.

[16] Robert D Richtmyer. Taylor instability in shock acceleration of compressible fluids. Technical report, Los Alamos Scientific Lab., N. Mex., 1954.

[17] Geoffrey Ingram Taylor. The instability of liquid surfaces when accelerated in a direction perpendicular to their planes. i. *Proceedings of the Royal Society of London. Series A. Mathematical and Physical Sciences*, 201(1065):192–196, 1950.

[18] Karnig O Mikaelian. Richtmyer-meshkov instabilities in stratified fluids. *Physical Review A*, 31(1):410, 1985.

[19] Robert C Cook, Randall L McEachern, and Richard B Stephens. Representative surface profile power spectra from capsules used in nova and omega implosion experiments. *Fusion technology*, 35(2):224–228, 1999.

[20] Marc A Meyers. *Dynamic behavior of materials*. John Wiley & Sons, 1994.

[21] Veselin A Dobrev, Tzanio V Kolev, and Robert N Rieben. High-order curvilinear finite element methods for lagrangian hydrodynamics. *SIAM Journal on Scientific Computing*, 34(5):B606–B641, 2012.

[22] VA Dobrev, TE Ellis, Tz V Kolev, and RN Rieben. Curvilinear finite elements for lagrangian hydrodynamics. *International Journal for Numerical Methods in Fluids*, 65(11-12):1295–1310, 2011.

[23] Robert W Anderson, Veselin A Dobrev, Tzanio V Kolev, Robert N Rieben, and Vladimir Z Tomov. High-order multi-material ALE hydrodynamics. *SIAM Journal on Scientific Computing*, 40(1):B32–B58, 2018.

[24] Robert W Anderson, Veselin A Dobrev, Tz V Kolev, and Robert N Rieben. Monotonicity in high-order curvilinear finite element arbitrary lagrangian–eulerian remap. *International Journal for Numerical Methods in Fluids*, 77(5):249–273, 2015.

[25] Antonio R Piriz, JJ Lopez Cela, Naeem A Tahir, and Dieter HH Hoffmann. Richtmyer-Meshkov instability in elastic-plastic media. *Physical Review E*, 78(5):056401, 2008.